RRKM Theory beyond the Separable Harmonic Approximation: The $HCO_2 \rightarrow H + CO_2$ Unimolecular Decomposition

Kurt M. Christoffel[†] **and Joel M. Bowman***

Department of Chemistry and Cherry L. Emerson Center for Scientific Computation, Emory University, Atlanta, Georgia 30322

Received: November 11, 1998; In Final Form: February 22, 1999

We report variational calculations of a large number of vibrational states of HCO_2 and the $H\cdots CO_2$ transition state for $J = 0$ using the code MULTIMODE and a realistic six degree-of-freedom potential energy surface. State-dependent rotational constants for both species are calculated for the same sets of vibrational states from exact rotation/vibration calculations for $J = 1$. The results of these variational calculations are used to obtain RRKM rate constants for the decomposition of HCO_2 to form $H + CO_2$. Comparison is made between these nonseparable RRKM results and those obtained from a standard, separable harmonic oscillator/rigid rotor evaluation of the RRKM rate constant expression. Significant differences between the nonseparable and separable results are found.

I. Introduction

Despite advances in computer technology in the past 2 decades, accurate quantum calculations of unimolecular and bimolecular reaction rate constants in systems with four or more atoms remain largely outside the realm of feasibility.[1,2] For such systems one must rely upon classical trajectory methods[3] or statistical theories, such as transition state theory (TST)[4,5] or RRKM theory,[6] to estimate elementary rate constants. Central to these statistical theories is an approximate calculation of the cumulative reaction probability (CRP), denoted $N(E)$ where E is the total energy. The CRP is defined as the sum of the state-to-state reaction probabilities summed over all initial and final states and it can be used to straightforwardly determine microcanonical and canonical rate constants.[7] In TST the exact $N(E)$ is approximated by the number of states of the transition state with energy less than or equal to E. Thus the dynamics calculation is replaced for a nonrotating N-atom system by a state count of the $(3N - 7)$−dimensional "bound" states of the transition state.

Routinely this state count is performed by invoking a further approximation that the vibrational degrees-of-freedom of the transition state are separable and harmonic. This form of TST is referred to as separable TST (STST). Before the advent of high-speed computing, this approach was defensible on the grounds that it was the only feasible approach given the era's typical dearth of ab initio data for stable molecules and even more so for transition states. However, now that chemically accurate potential energy surfaces can be developed for triatomic and tetraatomic systems, we must look beyond the standard approach to state counting to include the effects of anharmonicity and intermode coupling (i.e., nonseparability).

A limited amount of work has been done in the past 2 decades beyond this conventional approach. Garrett, Truhlar, and coworkers in a series of papers during the 1980s examined the effect of incorporating anharmonicity effects within separable oscillator models on TST rate constants for a series of A + BC reactions[8] and for the $OH + H_2$[9] reaction. Recently Isaacson[10] has generated a potential energy surface for the $OH + H_2$ reaction in the vicinity of the reaction path and then applied second-order perturbation theory and the self-consistent field configuration interaction (SCF-CI)[11] method to a quartic force field to obtain the anharmonic vibrational energy levels for the bound degrees-of-freedom orthogonal to the reaction coordinate. These levels, which include the effects of anharmonicity and mode−mode coupling, in many cases deviated significantly from their purely harmonic approximations. Miller and coworkers have developed and applied (to several reactions including the unimolecular decomposition of D_2CO) a nonseparable semiclassical TST (SCTST) approach to calculating $N(E)$ within a second-order perturbative treatment of anharmonicity for the determination of the good actions.[12] In a related development, Seideman and Miller have shown how the exact CRP can be evaluated directly (i.e., without calculation of the scattering matrix) using the normal coordinates of the transition state, including the imaginary-frequency mode.[13]

For unimolecular reactions, TST is combined with a statistical treatment of the energized reactant (based on the dynamical assumption of rapid intramolecular vibrational energy redistribution (IVR) relative to the reaction rate) in RRKM (or quasi-equilibrium) theory. RRKM theory gives a rate constant expression (neglecting for now the role of rotations) of the form[14]

$$k(E) = \frac{\sigma N^{\ddagger}(E)}{h\rho(E)} \tag{1}$$

where $\rho(E)$ is the density of vibrational states at the energy E (measured relative to the reagent zero-point energy), $N^{\ddagger}(E)$ is the total number (sum) of vibrational states in the transition state with energies not exceeding E and is given by

$$N^{\ddagger}(E) = \sum_n h(E - \epsilon_n^{\ddagger}) \tag{2}$$

* Author to whom correspondence should be addressed (bowman@euch3g.chem.emory.edu).

[†] Permanent address: Department of Chemistry, Augustana College, Rock Island, IL 61201-2296 (chchristoffel@augustana.edu).

10.1021/jp9843961 CCC: $18.00
Published on Web 04/02/1999

with h(x) being the Heaviside step function and $\{\epsilon_n^{\ddagger}\}$ being the set of transition state energy levels (measured relative to the zero-point energy of the reagent), and σ is the reaction symmetry factor. Application of RRKM theory to a particular reaction then involves, in addition to an approximate calculation of the CRP, the calculation of the density of states of the energized molecule at the relatively high energies typical of molecular bond breaking. Thus, incorporation of the effects of anharmonicity and intermode coupling into a calculation of $\rho(E)$ represents an even greater computational challenge than incorporating these effects for the transition state. This need for accurate densities of states to make RRKM theory quantitative has long been recognized.[5,6,15,16] Hase, Schinke, and coworkers recently determined essentially exact values (including effects of both anharmonicity and intermode coupling) of $N^{\ddagger}(E)$ and $\rho(E)$ for the decomposition of the nonrotating triatomic HO_2 radical.[17]

In this paper we apply nonseparable RRKM theory to the unimolecular decomposition of the tetraatomic HCO_2 radical to form H + CO_2, using a six degree-of-freedom potential[18] and including effects of rotation. Our calculations of the nonseparable bound states of the energized reactant and the transition state were done using the code MULTIMODE.[19] A summary of the theory and computational methods implemented within MULTIMODE is given in the next section along with the details of the utilization of its output for the current RRKM calculations. Section III presents our results with an emphasis on comparing them to the results obtained by application of separable RRKM theory (i.e., separable harmonic vibrations and a rigid rotator) to this reaction. In the final section we summarize our important findings and conclusions.

II. Theory and Computational Details

An exact evaluation of the quantities $N^{\ddagger}(E)$ and $\rho(E)$ used in the RRKM calculation of the microcanonical rate constant $k(E)$ requires a knowledge of the exact energy levels of the energized molecule and of the transition state species. Although the computation of the "exact" bound states of triatomic molecules has become almost routine,[20] the corresponding calculation for a polyatomic molecule (with four or more atoms) poses a formidable computational challenge. Such eigenvalue determinations are hampered by an essentially exponential scaling of the computational effort and resources required with the dimensionality (number of degrees of freedom) of the system whether a spectral (basis set expansion) or grid technique is employed. In the spectral approach the evaluation of the multidimensional integrals required in computing the potential contribution to the Hamiltonian matrix elements is very time-consuming and barely feasible even for tetraatomic molecules. For a grid representation of the Hamiltonian, on the order of 10^6 (or higher) points could be required for a tetraatomic molecule.

Thus to make such calculations tractable for polyatomic molecules we have advocated the use of the following hierarchical representation of the potential expressed in terms of mass-scaled normal modes[19]

$$V(Q_1,Q_2,...,Q_N) = \sum_i V_i^{(1)}(Q_i) + \sum_{ij} V_{ij}^{(2)}(Q_i,Q_j) + \sum_{ijk} V_{ijk}^{(3)}(Q_i,Q_j,Q_k) + \sum_{ijkl} V_{ijkl}^{(4)}(Q_i,Q_j,Q_k,Q_l) + ... \quad (3)$$

where $V_i^{(1)}(Q_i)$ is given by a cut through the potential along which only the coordinate Q_i is nonzero, $V_{ij}^{(2)}(Q_i,Q_j)$ is similarly defined but now the two coordinates Q_i and Q_j are nonzero, etc. The one-mode representation (1-MR) of the potential includes only the terms in the first sum above, the two-mode representation (2-MR) retains the terms in the first and second sums above, etc. Our applications to date[19] have been limited (by computational resources) to explicit coupling of a maximum of four modes. As a result, the calculations described in this paper involve at most four-dimensional quadratures. Although the method is not exact, we have found it to be capable of producing quite accurate results for tetraatomic molecules.[19c] (Note by way of contrast that in the standard separable TST/RRKM approach the potential is taken to be a harmonic 1-MR.)

The representation of the potential given by eq 3 can be incorporated into the full Watson normal-mode Hamiltonian (appropriate for nonlinear molecules) for which the kinetic energy operator is (in atomic units, $\hbar = 1$)[21]

$$\hat{T} = \frac{1}{2}\sum_{\alpha\beta}(\hat{J}_\alpha - \hat{\pi}_\alpha)\mu_{\alpha\beta}(\hat{J}_\beta - \hat{\pi}_\beta) - \frac{1}{2}\sum_k \frac{\partial^2}{\partial Q_k^{\,2}} - \frac{1}{8}\sum_\alpha \mu_{\alpha\alpha} \quad (4)$$

where $\hat{J}_\alpha$, $\hat{J}_\beta$ are components of the total angular momentum operator, $\hat{\pi}_\alpha$, $\hat{\pi}_\beta$ are components of the vibrational angular momentum operator, and μ is the inverse of the moment of inertia tensor. Explicitly,

$$\hat{\pi}_\alpha = -i\sum_{k,l} \zeta_{k,l}^{\alpha} Q_k \frac{\partial}{\partial Q_l} \quad (5)$$

where the $\zeta_{k,l}^{\alpha}$ are the Coriolis coupling constants, related to the vectors of the normal coordinates by

$$\zeta_{k,l}^{\alpha} = \epsilon_{\alpha\beta\gamma}\sum_i l_{\beta i,k} l_{\gamma i,l} \quad (6)$$

The mass-scaled normal coordinates Q_k are related to the Cartesian coordinates $r_{\alpha i}$ by

$$Q_k = \sum_i l_{\alpha i,k} m_i^{1/2}(r_{\alpha i} - r_{\alpha i}^0) \quad (7)$$

where $r_{\alpha i}^0$ are the equilibrium Cartesian coordinates in the principal axis system.

We have implemented the above approach for calculating rovibrational energy levels of polyatomic molecules at various levels of approximation in a new code called MULTIMODE.[19] This code can perform vibrational self-consistent field (VSCF) calculations and two types of configuration interaction (CI) calculations using the hierarchical representation of the potential, for $J > 0$. Molecular rotation can be treated exactly using the method of Whitehead and Handy[22] or approximately using the "adiabatic rotation approximation".[23]

In the VSCF approach[24] the vibrational wave function is assumed to be a "Hartree product" of one-mode functions $\phi_{n_i}^{(i)}(Q_i)$ known as "modals":

$$\Psi_{n_1,n_2,...,n_N}^{VSCF}(Q_1,Q_2,...,Q_N) = \prod_{i=1}^{N} \phi_{n_i}^{(i)}(Q_i) \quad (8)$$

Variational optimization of the modals to minimize the energy

yields (for the $J = 0$ Watson Hamiltonian) the following set of coupled integrodifferential VSCF equations

$$[T_l + \langle \prod_{i \neq l}^{N} \phi_{n_i}^{(i)}(Q_i) | V + T_c | \prod_{i \neq l}^{N} \phi_{n_i}^{(i)}(Q_i) \rangle - \epsilon_{n_l}^{(l)}] \phi_{n_l}^{(l)}(Q_l) = 0 \qquad l = 1, ..., N \quad (9)$$

where V is an n-mode representation of the potential ($n = 1$, 2, 3, 4), T_c is the Coriolis coupling operator, and T_l is the Cartesian kinetic energy operator for mode l in the Watson Hamiltonian.

These equations are solved iteratively starting with zero-order, normal-mode, harmonic oscillator wave functions as initial "guesses" for the modals. For the $J = 0$ results discussed in section III, the set of equations (9) was solved for the SCF ground state, $\{n_i\} = \{0\}$, until the corresponding eigenvalues from successive iterations had converged to within 0.01 cm^{-1}. (For both HCO_2 and the transition state this criterion was satisfied in three iterations.)

In addition, at the end of the VSCF calculation a set of converged ground state VSCF 1-mode Hamiltonians (analogous to converged one-electron Fock operators but without exchange terms) collectively referred to as the VSCF Hamiltonian is obtained. Excited eigenstates of this VSCF Hamiltonian, known as virtual states, can be generated and used as a basis for a configuration interaction procedure to obtain variational results which converge to exact results (for the chosen representation of the potential). Since the members of this basis form an orthonormal set, a standard eigenvalue problem, $\mathbf{H}^{VCI}\mathbf{C} = E\mathbf{C}$, results and is solved using standard software. This type of CI procedure which we term "VCI" is the one used in obtaining the "CI" results of section III, [MULTIMODE is also capable of performing a CI calculation using a basis of true SCF states which results in a generalized eigenvalue problem $(\mathbf{H}^{SCF} - E\mathbf{S})C = 0$, where $\mathbf{S}$ is the overlap matrix for the SCF states.] In the present ($J = 0$) calculations, the CI matrix was generated by fixing the TOTAL quanta of mode excitations in the virtual states of the basis to be less than or equal to a maximum value, $n_{max} = 6-10$ here.

The application of MULTIMODE to a transition state is straightforward, since in this case one of the normal modes corresponds to an imaginary-frequency, reaction coordinate mode. If that mode is eliminated, the resulting Hamiltonian is one representing the "bound" states of the transition state. The construction and diagonalization of the Hamiltonian in $3N - 7$ modes using MULTIMODE then proceeds as usual, and the nonseparable quantized states of a transition state can be obtained. An application of MULTIMODE to the calculation of the quantized nonseparable states of the transition state of the $OH + H_2$ reaction has already been done.[25]

In calculations with $J > 0$, the MULTIMODE code utilizes the exact Whitehead−Handy implementation of Watson's rovibrational kinetic energy operator for nonlinear molecules.[22] For a given J value, $(2J + 1)$ "vibrational" calculations are carried out for each of the $(2J + 1)$ pairs of the quantum numbers (K_a,K_c) to form the $(2J + 1)$ diagonal blocks of the rovibrational Hamiltonian matrix, and then the remaining nonzero blocks are filled in appropriately. In doing so we use the same VCI vibrational basis for each K block multiplied by the appropriate combination of symmetric top rotational functions. Since our vibrational basis is the same for all K blocks, we need to evaluate the matrix elements as functions of the vibrational coordinates only once and then repeatedly multiply each matrix element by the appropriate pure rotational matrix element to form complete rovibrational Hamiltonian matrix elements. The rovibrational Hamiltonian is then diagonalized using a Givens method to obtain the rovibrational energies. Further details of these procedures including analytical expressions for the nonzero pure rotational matrix elements have been given elsewhere.[19c] The "adiabatic rotation approximation",[19b] an efficient approximate treatment of rotation, can also be done in MULTIMODE, and we present limited results using this approximation and compare them to the exact ones below.

TABLE 1: Properties of Stationary Points for $HCO_2 \rightarrow H + CO_2$

	HCO_2	$H\cdots CO_2$	$H + CO_2$
energy (eV)	0	0.70	0.15
energy (cm^{-1})	0	5635	1193
R_{CH} (a_o)	2.09	3.82	∞
$R_{CO,CO'}$ (a_o)	2.40, 2.40	2.27, 2.27	2.19, 2.19
θ_{HCO} (deg)	117.9	99.0	
$\theta_{OCO'}$ (deg)	124.1	161.9	180.0
NM frequencies (cm^{-1})	549, 1009, 1057, 1449, 1919, 3108	404i, 254, 420, 575, 1149, 2152	743, 1351, 2384

The potential used in this study is the latest version of the HCO_2 surface developed by Schatz and co-workers.[18] This surface is based on a many-body expansion where the two- and three-body terms come from known potential surfaces for HCO, HO_2, and CO_2 and the four-body terms were determined from a fit of ab initio data. HCO_2 occurs as a local minimum on this surface along one of two minimum energy pathways connecting the $OH + CO$ and $H + CO_2$ asymptotes. However, due to a rather large barrier to formation of HCO_2 (from $OH + CO$), this pathway is not expected to be significant at thermal energies. However, the objective of this study is not a complete description of the full $OH + CO \rightarrow H + CO_2$ system. Instead we focus on the $HCO_2 \rightarrow H + CO_2$ step as a typical tetraatomic system for which a realistic potential energy surface is available, as indicated by the semiquantitative agreement between dynamics calculations on this surface and experiment. We then investigate the differences that arise between applications of separable harmonic RRKM theory and nonseparable RRKM theory to this "model" reaction. For completeness, Table 1 gives the geometries, energetics, and normal mode frequencies of HCO_2, the $H\cdots CO_2$ transition state, and the $H + CO_2$ products. (Energies there are referenced to the HCO_2 minimum taken as zero.) It is worth noting that the value of the imaginary "reaction coordinate" frequency at the saddle point in this fit is 404i cm^{-1}, substantially different from that in earlier versions of this surface (239i and 280i cm^{-1}) and from the ab initio estimate (1147i cm^{-1}). As we will see in section 3 below, the magnitude of this frequency may significantly affect the importance of tunneling for this reaction.

III. Results and Discussion

A. $J = 0$. In separable RRKM theory, the quantities $N^{\ddagger}(E)$ and $\rho(E)$ are obtained using (separable) normal mode harmonic energies. For the HCO_2 minimum and the $H\cdots CO_2$ transition state, we have determined the normal mode frequencies and eigenvectors by diagonalization of the matrix of Cartesian potential energy second derivatives (evaluated numerically using a standard central difference formula). These frequencies are given in Table 1 and the corresponding eigenvectors are illustrated in Figures 1 and 2, for HCO_2 and $H\cdots CO_2$, respectively. These normal mode frequencies were used to generate harmonic spectra which were used to determine $N_{HO}(E)$ and $N_{HO}^{\ddagger}(E)$ for HCO_2 and the $H\cdots CO_2$ transition state, respectively, by direct count. In the energy range ap-

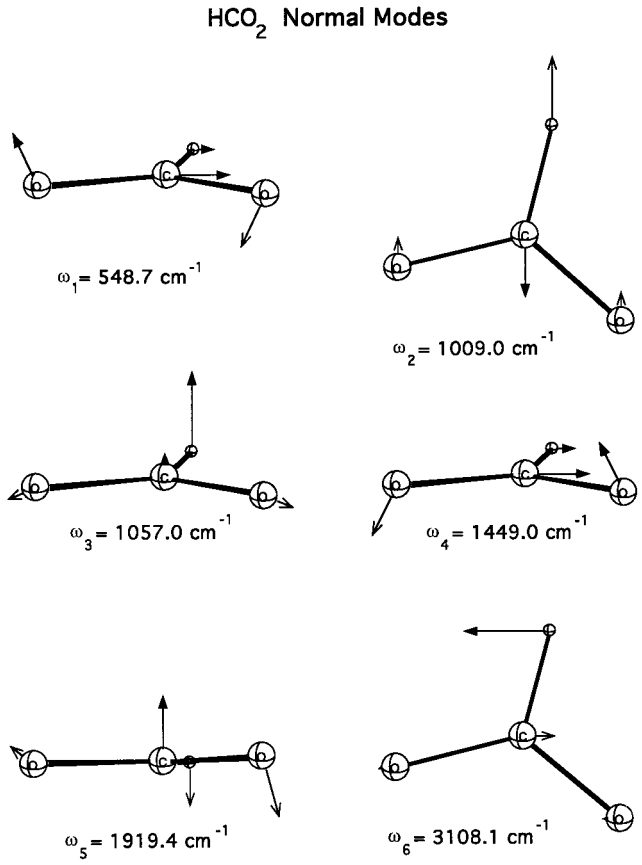

Figure 1. Normal mode eigenvectors for HCO_2.

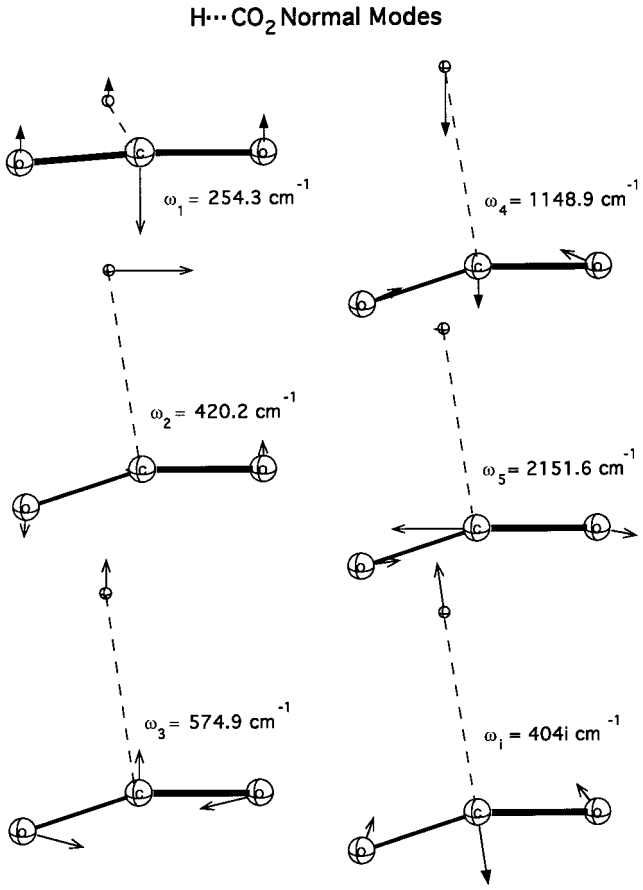

Figure 2. Normal mode eigenvectors for the H···CO_2 transition state.

proximately 3000 cm^{-1} above threshold $N_{HO}(E)$ was fit to a cubic polynomial. [Our findings were that in all the cases described in this paper the "goodness" of cubic polynomial fits to $N_{HO}(E)$ and the nonseparable $N(E)$ (described later below) surpassed that of power law fits as measured by the closeness of the linear correlation coefficient to unity.] The derivative of this cubic fit was performed to obtain an analytical expression for $\rho_{HO}(E)$.

To obtain anharmonic nonseparable values for $N(E)$ and $N^{\ddagger}(E)$ the MULTIMODE code was used to generate large numbers of energy levels for HCO_2 and the H···CO_2 transition state using 3-mode and 4-mode representations of the potential. The primitive basis sets used to generate the VSCF virtual states employed in the VCI calculations for HCO_2 typically consisted of 12−16 functions for normal modes 1−3 and of 9−13 functions for normal modes 4−6. In the case of H···CO_2, the primitive basis sets consisted of 15 functions for normal modes 1 and 2 and typically 8−10 (although 15 were employed in one calculation) functions for normal modes 3−5. The largest 4-MR calculations for HCO_2 correspond to $n_{max} = 8$, which results in a CI matrix of order 3003; the largest 3-MR calculations for HCO_2 correspond to $n_{max} = 10$ and a CI matrix of order 8008. For the H···CO_2 calculations the largest value of n_{max} used, 8, results in a CI matrix of order 1287. The smaller values of n_{max} and of the number of primitive basis functions used for the H···CO_2 calculations are justified by the fact that our RRKM calculations are limited to energies no more than 3000 cm^{-1} above the zero point energy (ZPE) level of the transition state. (This level of excitation though is nearly 6500 cm^{-1} above the ZPE of HCO_2.)

The results of these VCI calculations are shown in Table 2 for some of the low-lying states of HCO_2. A comparison of the first two columns (of energies) in Table 2 indicates that the general effect of the inclusion of the additional terms in a 4-MR of the potential for this system is to slightly raise the energy levels. In general, the agreement between these two calculations with identical bases is good, with most levels agreeing to within 10 cm^{-1} (which is small compared to the average level spacing). Those 4-MR results represent our largest calculation for HCO_2 and took about 51 h of central processing unit (CPU) time

TABLE 2: Low-Lying Energy Levels (cm^{-1}) of HCO_2

$\nu_1\nu_2\nu_3\nu_4\nu_5\nu_6$	4-MR[a]	3-MR[a]	3-MR[b]	3-MR[c]
ZPE	4673.4	4672.1	4672.8	4672.7
1 0 0 0 0 0	414.41	413.46	413.15	413.06
2 0 0 0 0 0	773.85	771.43	770.17	769.64
0 1 0 0 0 0	859.66	856.83	856.56	856.33
3 0 0 0 0 0	1107.2	1103.5	1098.2	1095.4
1 1 0 0 0 0	1203.1	1197.8	1195.6	1194.3
0 0 0 1 0 0	1284.9	1282.7	1281.9	1281.8
2 1 0 0 0 0	1475.1	1471.6	1459.8	1452.5
4 0 0 0 0 0	1508.1	1501.0	1490.5	1483.8
1 0 0 1 0 0	1631.4	1627.9	1624.8	1623.4
0 2 0 0 0 0	1664.9	1657.9	1654.8	1653.0
0 0 0 0 1 0	1801.4	1798.0	1797.3	1797.3
3 1 0 0 0 0	1848.3	1841.5	1820.2	1805.3
5 0 0 0 0 0	1907.8	1904.8	1882.9	1868.6
0 0 0 0 0 1	1903.2	1920.2	1879.4	1873.5
0 0 1 0 0 0	1919.2	1900.2	1897.5	1897.3
1 2 0 0 0 0	1936.5	1930.3	1914.6	1903.4
2 0 0 1 0 0	1964.7	1958.5	1950.0	1946.2
0 1 0 1 0 0	2081.0	2067.8	2064.2	2062.6
1 0 0 0 1 0	2181.9	2176.7	2175.6	2175.2
2 2 0 0 0 0	2253.8	2246.4	2214.2	2189.7
4 1 0 0 0 0	2260.7	2254.9	2218.6	2196.0
1 0 1 0 0 0	2290.6	2281.4	2276.9	2276.2
VSCF ZPE	4688.0	4687.1	4687.9	4686.1

[a] $n_{max} = 8$, dimension of $\mathbf{H}^{VCI} = 3003$. [b] $n_{max} = 9$, dimension of $\mathbf{H}^{VCI} = 5005$. [c] $n_{max} = 10$, dimension of $\mathbf{H}^{VCI} = 8008$.

on an SGI Indigo 2 with a MIPS R8000 processor. The corresponding 3-MR calculation required just over 1 h of CPU time on the same machine. In light of the considerably greater computational effort required and the rather modest improvements offered by the 4-MR calculations, we limited our larger VCI calculations ($n_{max} = 9,10$) for HCO_2 to those using the 3-MR of the potential. The larger of these two 3-MR calculations required about 22 h of CPU time. Most levels appear to be converged to within about 15 cm^{-1} (and many exhibit much better convergence). As our ultimate aim is for a reasonable estimate of the density of states for HCO_2 above the threshold for formation of $H + CO_2$ and not for spectroscopic accuracy, we feel that the level of convergence of these results is sufficient.

One major conclusion that we can reach by examination of the results in Table 2 and of the normal mode frequencies for HCO_2 given in Table 1 is that anharmonicity and intermode coupling are important in HCO_2, even at relatively low levels of excitation. All of the MULTIMODE calculations give a ZPE in the range of 4671−4674 cm^{-1}, while the harmonic NM ZPE is 4545.6 cm^{-1}, a difference of over 125 cm^{-1}. A greater appreciation of the importance of these two effects is gained by comparison between the MULTIMODE and NM fundamental excitation energies which on average deviate by 442 cm^{-1}, corresponding to an average relative deviation of about 30%. The differences are most pronounced for normal modes 3 and 6. In the former case, the nonseparable excitation energy is nearly twice the NM excitation energy (1900 versus 1057 cm^{-1}, respectively). The mode 6 nonseparable excitation energy is substantially lower (about 1200 cm^{-1}) than its NM counterpart. These two effects can be largely (but not exclusively) attributed to "diagonal" anharmonicity, as indicated by results of 1-MR calculations for HCO_2 (which include no intermode coupling), which yield fundamental excitation energies of 2069.5 and 2340.2 cm^{-1} for modes 3 and 6, respectively. The sizable differences between these 1-MR (separable anharmonic) results and the 3-MR results indicate that intermode coupling is substantial. Fundamental excitation energies calculated using a 1-MR (which includes diagonal anharmonicity but not intermode coupling) differ on average from the nonseparable excitation energies by 202 cm^{-1}, indicating clearly that, even at these low levels of excitation, intermode coupling is significant in HCO_2. From these results it should be obvious that inclusion of *both* anharmonicity and intermode coupling into calculations of the numbers and densities of states are crucial for accurate applications of RRKM theory in this system.

Several sets of 4-MR VCI results and our largest 3-MR VCI results for the low-lying states of the H···CO_2 transition state are given in Table 3. Comparison of the energies from the largest 3-MR and 4-MR calculations shows the two sets of results to be very close with the energies for *most* states differing by less than 3 cm^{-1}. As for HCO_2, the 4-MR energies are generally slightly higher than the 3-MR energies. Comparison of the three sets of 4-MR results (for different basis sets of virtual states) indicates that all of the energy levels shown are probably converged to within 5 cm^{-1}, with the first dozen lowest levels being converged to within 1 cm^{-1}. As for HCO_2, the nonseparable and NM zero point energies are substantially different, with the NM ZPE about 250 cm^{-1} below the nonseparable ZPE (2275 versus 2523 cm^{-1}). The differences between the nonseparable and NM excitation energies are overall smaller than for HCO_2. The average deviation between these two sets of results for the five modes is 122 cm^{-1}, corresponding to an average relative deviation of 17%. (The nonseparable excitation energy for mode 5 not shown in Table 3 is 2219.5 cm^{-1}.) However, the nonseparable excitation energy for mode 2 is essentially double the NM value (840.3 versus 420.2 cm^{-1}). (Most of this effect is the result of "diagonal" anharmonicity; a 1-MR calculation gives a fundamental excitation energy for this mode of 822.0 cm^{-1}.) A comparison between nonseparable and 1-MR fundamental excitation energies for the H···CO_2 transition state shows that on average the two sets of results differ by only 13 cm^{-1}, indicating that at these levels of excitation diagonal anharmonicity is the dominant effect neglected in a NM treatment of the transition state. This further suggests that 1-MR results might provide a reasonable approximation to $N^{\ddagger}(E)$ in this system.

TABLE 3: Low-Lying Energy Levels (cm^{-1}) of H···CO_2

$\nu_1\,\nu_2\,\nu_3\,\nu_4\,\nu_5$	4-MR[a]	4-MR[b]	4-MR[c]	3-MR[c]
ZPE	2523.3	2523.3	2523.3	2523.1
1 0 0 0 0	365.28	365.24	365.22	364.95
0 0 1 0 0	568.42	568.26	568.18	567.56
2 0 0 0 0	761.64	761.46	761.39	760.91
0 1 0 0 0	840.39	840.34	840.33	840.14
1 0 1 0 0	930.97	930.43	930.18	928.62
0 0 2 0 0	1123.7	1122.2	1121.2	1119.1
0 0 0 1 0	1155.6	1155.3	1155.1	1154.6
3 0 0 0 0	1171.3	1170.0	1169.8	1169.1
1 1 0 0 0	1225.8	1225.7	1225.6	1225.1
2 0 1 0 0	1330.8	1328.7	1328.0	1325.9
0 1 1 0 0	1428.1	1427.7	1427.5	1426.4
1 0 2 0 0	1488.1	1483.3	1481.1	1476.4
1 0 0 1 0	1537.4	1536.7	1536.4	1535.5
4 0 0 0 0	1596.7	1589.1	1587.3	1586.4
2 1 0 0 0	1634.9	1633.9	1633.7	1632.8
0 0 3 0 0	1668.9	1653.5	1645.5	1637.7
0 0 1 1 0	1679.3	1677.9	1677.2	1675.6
0 2 0 0 0	1705.5	1705.0	1704.7	1704.5
3 0 1 0 0	1747.1	1738.9	1736.0	1733.2
1 1 1 0 0	1814.4	1812.6	1812.2	1809.9
2 0 2 0 0	1898.6	1888.6	1883.2	1877.8
2 0 0 1 0	1945.8	1943.4	1942.6	1941.5
0 1 0 1 0	1968.7	1967.3	1966.8	1965.7
VSCF ZPE	2528.1	2528.1	2528.1	2528.0

[a] $n_{max} = 6$, dimension of $\mathbf{H}^{VCI} = 462$. [b] $n_{max} = 7$, dimension of $\mathbf{H}^{VCI} = 792$. [c] $n_{max} = 8$, dimension of $\mathbf{H}^{VCI} = 1287$.

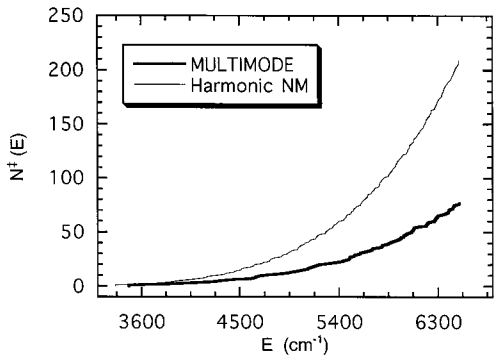

Figure 3. Separable harmonic and nonseparable VCI sums of states at the H···CO_2 transition state for $J = 0$. In this and all subsequent figures, E is the energy in excess of the HCO_2 zero-point energy.

Given the excellent convergence of the 4-MR calculations for H···CO_2, $N^{\ddagger}(E)$ was determined by direct count of the results from our largest ($n_{max} = 8$) 4-MR calculation. Figure 3 presents a comparison between the nonseparable $N^{\ddagger}(E)$ and $N^{\ddagger}_{HO}(E)$. There are two notable differences between these two quantities. First $N^{\ddagger}_{HO}(E)$ becomes nonzero about 120 cm^{-1} lower than does $N^{\ddagger}(E)$, a result of the difference between the nonseparable and NM zero point energies described above. Second at all energies shown, $N^{\ddagger}_{HO}(E) \geq N^{\ddagger}(E)$; in fact, at the highest energy

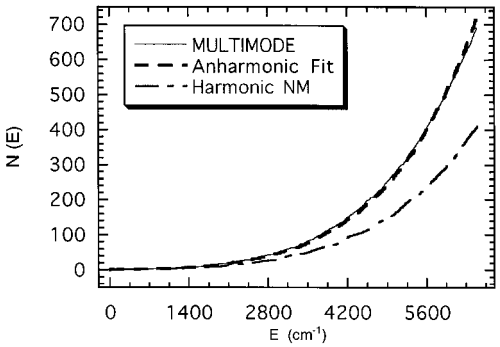

Figure 4. Separable harmonic, anharmonic fit, and nonseparable VCI sums of states for HCO_2 for $J = 0$.

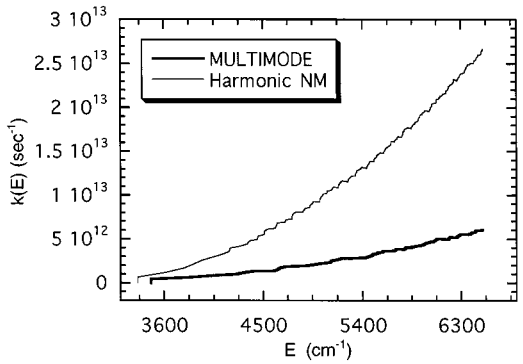

Figure 5. Separable harmonic and nonseparable VCI microcanonical rate constants $k(E)$ for dissociation of HCO_2 to form $H + CO_2$ for $J = 0$.

shown (about 6500 cm^{-1}), the difference is nearly a factor of 3. Thus a harmonic count appreciably overestimates the numerator of the RRKM rate constant expression (eq 1) for this reaction.

Because of the relatively high levels of excitation of the low-frequency modes of HCO_2 possible at and beyond the reaction threshold and because of the limitations on our basis sets imposed by the computer memory available, we had some doubts as to the completeness of our spectrum for HCO_2 above threshold. We decided to test the spectral completeness by modeling HCO_2 as a system of six separable anharmonic oscillators. Each oscillator was assumed to have a Birge−Sponer spectrum with energy levels labeled by the vibrational quantum number v_i.

$$E_{v_i} = c_i + a_i\left(v_i + \frac{1}{2}\right) + b_i\left(v_i + \frac{1}{2}\right)^2 \qquad (10)$$

The parameters a_i, b_i, and c_i for each oscillator were determined by optimizing the fit of eq 10 to MULTIMODE (coupled) results for a progression of single-mode excitation energy levels. A direct count procedure was then used to generate an independent anharmonic oscillator spectrum and the corresponding "anharmonic fit" to the sum of states $N_{anh}(E)$. In Figure 4 we show a comparison of the anharmonic fit, harmonic normal mode, and nonseparable MULTIMODE results for $N(E)$. The first thing to notice is that the MULTIMODE-based results are in rather close agreement with the anharmonic fit over the whole energy range of interest. In the energy range up to 5000 cm^{-1}, where we are confident that the spectrum we have calculated is complete, the anharmonic fit is typically lower than the nonseparable value of $N(E)$ by no more than 5%. This might have been anticipated as a result of intermode coupling which is only indirectly built into the anharmonic fit. As the energy is increased beyond 5000 cm^{-1}, these two curves cross. We feel that this behavior indicates a slight incompleteness of our spectrum, probably on the order of 10% missing levels or less at the highest energy shown. The most striking feature of Figure 4 is that in the energy regime beyond threshold (above 3500 cm^{-1}) the harmonic NM approximation for $N(E)$, $N_{HO}(E)$, is noticeably smaller than the nonseparable result for $N(E)$, by as much as a factor of 1.5 at the high end of the energy range. [If our conjecture about the incompleteness of the computed nonseparable spectrum is correct, the discrepancy between the true number of states and $N_{HO}(E)$ is even greater than indicated in the figure.] Thus the HCO_2 system seems to show the typical molecular behavior, i.e., the separable harmonic number (and density) of states is less than the coupled anharmonic number (and density) of states.[26] Thus a harmonic NM approximation noticeably underestimates $\rho(E)$ in the denominator of the RRKM rate constant expression (eq 1). For example, at $E = 5000$ cm^{-1} (about midway through the reactive energy range) $\rho_{HO}(E) = 0.1093/cm^{-1}$ while the nonseparable value of $\rho(E)$ is $0.1909/cm^{-1}$. For the RRKM calculations reported below, we have fit our largest 3-MR results for the sum of states $N(E)$ to a cubic polynomial and differentiated this fit to obtain an analytical expression for $\rho(E)$.

Figure 5 shows the RRKM microcanonical rate constant $k(E)$ for $HCO_2 \rightarrow H + CO_2$ ($J = 0$) computed using both our MULTIMODE results and the separable harmonic NM results for $\rho(E)$ and $N^{\ddagger}(E)$. As might have been anticipated from the comments above, the harmonic threshold is about 120 cm^{-1} lower, and at all energies, the harmonic results exceed the nonseparable results, by more than a factor of 4 at the highest energy considered. Figure 5 dramatically emphasizes one of the major conclusions of this paper: that we must go beyond the usual harmonic NM approximation if we hope to achieve quantitative accuracy using RRKM theory.

As this reaction involves the breaking of a weak C−H bond, it would be expected that the reaction coordinate motion would entail primarily separation of the H atom from the center-of-mass of CO_2. This is confirmed in Figure 2, which shows that the imaginary-frequency NM approximation to the reaction coordinate consists primarily of this motion, plus bending motion that will bring the CO_2 moiety of the transition state into the characteristic collinear geometry of the CO_2 product. Due to the significance of hydrogen motion along the reaction coordinate, we would expect that tunneling effects might be important below the classical threshold for this reaction. As Miller has noted,[27] the only *simple* way to include tunneling into RRKM theory involves the further dynamical approximation of separability of the reaction coordinate from the other degrees of freedom. In such an approximate separable treatment, tunneling effects are taken into account by replacing the Heaviside step functions in the sum of states (eq 2) by one-dimensional tunneling probabilities, $P(E-\epsilon_n^{\ddagger})$, where $\epsilon_n^{\ddagger}$ are the nonseparable energy levels of the transition state. In the classical limit $P(E-\epsilon_n^{\ddagger}) \rightarrow h(E-\epsilon_n^{\ddagger})$ and RRKM theory without tunneling is recovered.

To gain some insight into the significance of tunneling in this reaction, we have incorporated such one-dimensional tunneling probabilities into our nonseparable RRKM calculations. We have represented the potential along the reaction coordinate as a generalized Eckart potential[28] using parameters consistent with the ground state vibrationally adiabatic effective potential for the system. In this case the "RRKM plus tunneling" approximations to $N^{\ddagger}(E)$ will reduce in the classical limit to the RRKM results without tunneling. The Eckart potential is

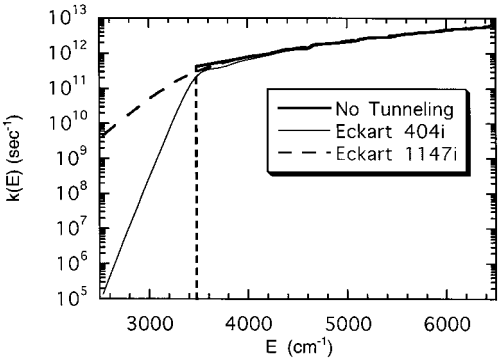

Figure 6. Nonseparable VCI microcanonical rate constants $k(E)$ for $HCO_2 \rightarrow H + CO_2$ dissociation including separable Eckart tunneling correction for $J = 0$. Short dashed vertical line indicates classical threshold energy.

characterized by three parameters: V_0 and V_1, the barrier heights in the forward and reverse directions, respectively, and ω_b, the absolute value of the imaginary barrier frequency, which is related to the potential curvature at the top of the barrier. The tunneling probability for this barrier can be evaluated analytically as[27]

$$P(E') = \frac{\sinh a \sinh b}{\sinh^2\left(\frac{a+b}{2}\right) + \cosh^2 c} \tag{11}$$

where

$$a = \frac{4\pi}{\hbar\omega_b}\frac{\sqrt{E' + V_0}}{[V_0^{-1/2} + V_1^{-1/2}]}$$

$$b = \frac{4\pi}{\hbar\omega_b}\frac{\sqrt{E' + V_1}}{[V_0^{-1/2} + V_1^{-1/2}]}$$

$$c = 2\pi\sqrt{\frac{V_0 V_1}{(\hbar\omega_b)^2} - \frac{1}{16}}$$

and where $E' = 0$ at the top of the barrier. V_0 and V_1 are simply the forward and reverse barrier heights along the ground state vibrationally adiabatic barrier. The exact value of ω_b appropriate for this reaction is an unresolved issue. The Bradley−Schatz version of the potential[18] gives a value of 404 cm^{-1}, which is substantially different from the original ab initio estimate of 1147 cm^{-1}. Thus we have performed two sets of "RRKM plus tunneling" calculations corresponding to these two very different values of ω_b. Figure 6 shows our results for the microcanonical rate constant $k(E)$ using our nonseparable results for $\rho(E)$ and $N^{\ddagger}(E)$ and including this approximate separable treatment of tunneling. Obviously at energies above the classical threshold, tunneling effects quickly become inconsequential. From Figure 6 it is clear that, below threshold, tunneling can produce rather sizable dissociation rates. This is particularly true for $\omega_b = 1147$ cm^{-1}, as would be expected, since larger values of ω_b correspond to greater curvature and hence, for fixed V_0 and V_1, a narrower potential barrier. Also worth noting is the logarithmic scale of Figure 6; the predictions for the two values of ω_b differ by orders of magnitude just 500 cm^{-1} below the classical threshold. This underscores the sensitivity of tunneling corrections to properties of the potential energy surface in the saddle point region.

Finally it is worth noting the implications of our results for a TST calculation of the rate of the $H + CO_2$ recombination reaction in the high pressure limit. The TST theory expression for this rate constant is

$$k_{rec}(T) = \frac{k_B T}{h}\frac{Q^{\ddagger}(T)}{Q_r(T)} e^{-E^{\ddagger}/k_B T} \tag{12}$$

where $Q^{\ddagger}(T)$ and $Q_r(T)$ are the partition functions of the transition state and the $H + CO_2$ reactants, respectively, k_B is the Boltzmann constant, and $E^{\ddagger}$ is the threshold energy on the ground state vibrationally adiabatic potential, i.e., the energy difference between the ZPE of the transition state and the ZPE of the CO_2 reactant. As we have noted above, the separable harmonic approximation underestimates the ZPE of the H···CO_2 transition state by about 250 cm^{-1}. The separable harmonic approximation *overestimates* the CO_2 ZPE by on the order of 50 cm^{-1}. The net result is that the separable harmonic approximation predicts a threshold energy about 300 cm^{-1} lower than a nonseparable treatment. At 300 K this difference in threshold energies alone would cause the separable harmonic approximation to overestimate $k_{rec}(T)$ by a factor of 4.2. Additionally since $N^{\ddagger}(E)$ from the separable approximation increases much more rapidly with energy than the nonseparable result for $N^{\ddagger}(E)$ (as seen in Figure 3), we can expect that the separable approximation to $Q^{\ddagger}(T)$ will generally exceed the accurate nonseparable value. Further if CO_2 shows typical molecular behavior, the separable approximation will underestimate the value of $Q_r(T)$. These two effects will increase the discrepancy between the separable harmonic approximation to $k_{rec}(T)$ and the accurate nonseparable result for $k_{rec}(T)$.

B. J > 0. Inclusion of rotation into a quantum problem greatly increases the computational resources required for solving that problem, since the number of relevant internal states grows like $(2J + 1)$ compared to the $J = 0$ case. As a result, our $J > 0$ calculations have been rather limited particularly for HCO_2 with an additional vibrational degree of freedom and for which we need to consider much greater internal energies as compared to the H···CO_2 transition state. For the H···CO_2 transition state we have been able to easily perform 3-MR $n_{max} = 8$ calculations including an exact treatment of rotation for $J = 1$, 5, 10 (using just over 100 MB of memory and less than 5 h of CPU time). However, our single 3-MR calculation for HCO_2 with $n_{max} = 9$, $J = 1$, using an exact treatment of rotation required just over 400 MB of memory and slightly more than 25 h of CPU time.

Computational limitations dictate that the most feasible treatment of rotational effects will be an approximate one, preferably one that makes maximum use of our limited amount of data based on an exact treatment of rotation. The exact calculations (within a given n-MR of the potential; in all cases below $n = 3$) yield rovibrational energies which can be labeled by the usual spectroscopic quantum numbers K_a and K_c. Both HCO_2 and the H···CO_2 transition state are near prolate symmetric tops; the asymmetry splittings are relatively small for $J = 1$: less than 0.05 cm^{-1} for all but one state of H···CO_2 and less than 0.1 cm^{-1} for all but 15 of over 600 accessible vibrational states of HCO_2, with none of these splittings greater than 0.2 cm^{-1}. The equilibrium geometry rigid rotor constants A_e, B_e, and C_e are 3.105, 0.420, and 0.370 cm^{-1}, respectively, for HCO_2, and 3.445, 0.373, and 0.337 cm^{-1}, respectively, for the H···CO_2 transition state. These constants correspond to values of Ray's asymmetry parameter of −0.963 and −0.977, respectively for HCO_2 and the transition state, quite close to the prolate symmetric top limit of −1. Thus we have chosen to model each of these species as a prolate symmetric top. The differences between the $J = 0$ and $J = 1$ "exact" (within the same 3-MR of the potential and using the same value of

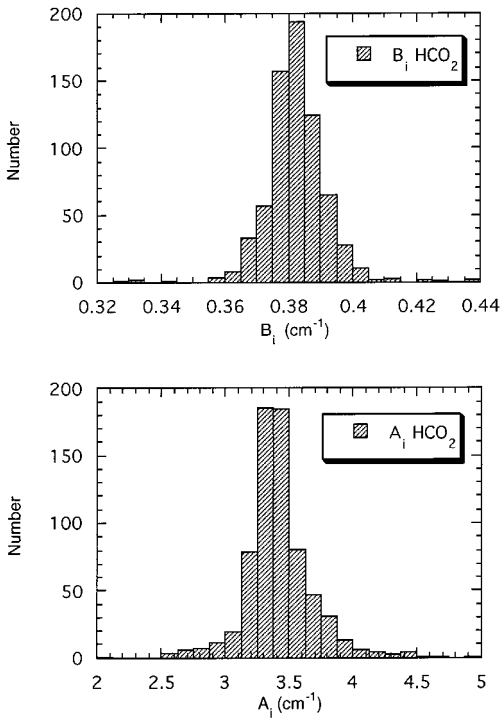

Figure 7. Distribution of state-specific rotational constants A_i and B_i for HCO_2. For comparison, the equilibrium geometry rotor constants A_e, B_e, and C_e are 3.105, 0.420, and 0.370 cm^{-1}, respectively.

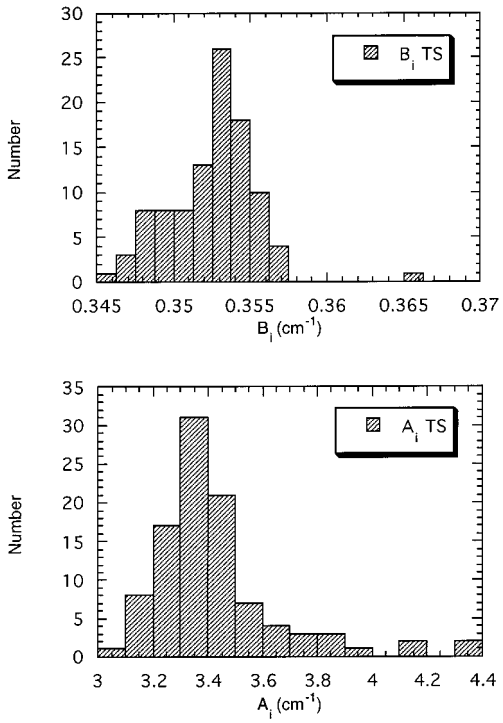

Figure 8. Distribution of state-specific rotational constants A_i and B_i for the H···CO_2 transition state. For comparison, the equilibrium rotor constants A_e, B_e, and C_e are 3.445, 0.373, and 0.337 cm^{-1}, respectively.

n_{max}) energies for a vibrational state i were fit to the standard prolate symmetric top expression

$$\Delta E^{(i)}_{J,K_a} = B_i J(J+1) + (A_i - B_i)K_a^2 \qquad (13)$$

to determine for each vibrational state effective rotational constants A_i and B_i. Use of the preceding rotational energy expression assumes that to a good approximation rotation and vibration are nearly separable.

Using the fitting procedure described above, constants A_i and B_i were determined for 700 vibrational states of HCO_2 and for 100 vibrational states of the H···CO_2 transition state. (These totals include 61 states for HCO_2 and 23 states for H···CO_2 which are beyond the range of energies for which we report RRKM rate constants.) For HCO_2 the average over states i of A_i denoted $\langle A_i \rangle$, is 3.413 cm^{-1}, and the average value of B_i, $\langle B_i \rangle$, is 0.382 cm^{-1}. The mean deviations from these average values are 0.225 cm^{-1} and 0.007 cm^{-1} for A_i and B_i, respectively. For the H···CO_2 transition state $\langle A_i \rangle = 3.436$ cm^{-1} and $\langle B_i \rangle = 0.353$ cm^{-1}. The corresponding mean deviations are 0.165 and 0.002 cm^{-1} for A_i and B_i, respectively. The averages are very close to the equilibrium geometry values with the exception of $\langle A_i \rangle$ for HCO_2, which differs from the equilibrium geometry value by about 10%. Figures 7 and 8 show histogram representations of the distributions of B_i and A_i values for HCO_2 and for the H···CO_2 transition state, respectively. These histograms are based on all of the available data with the exception of A_i for HCO_2, where a small number of values ($\approx$2% of the total) lying outside the range of 2−5 cm^{-1} have been omitted. Both B_i distributions are quite narrow; the A_i distributions are much broader, particularly the one for HCO_2 which exhibits rather long tails.

These sets of A_i and B_i values can be used to construct approximate rovibrational spectra (for both HCO_2 and the transition state) in the following manner. First we assume that the state-specific rotational constants are independent of J for $J > 1$; i.e., they are true constants as for a semirigid body. We further assume that rotation and vibration are approximately separable so that the rovibrational energy levels are given by

$$E^{(i)}_{J,K_a} = E^{(i)}_{J=0} + \Delta E^{(i)}_{J,K_a} \qquad (14)$$

where $\Delta E^{(i)}_{J,K_a}$ is given by eq 13. For a specified value of total angular momentum J, an approximate rovibrational spectrum is generated by evaluation of eq 14 for each of the $(2J + 1)$ values of K_a for each of the available $J = 0$ vibrational states i.

For the H···CO_2 transition state, we have been able to test the quality of these approximate spectra for $J = 5$, 10. For $J = 5$, we compared the 1078 lowest rovibrational energies from the fit described above to exact results (working for consistency within the same 3-MR of the potential and using data obtained from MULTIMODE calculations using the same value of n_{max}, 8). The average deviation between corresponding levels is 0.252 cm^{-1}. Over 90% of the energy levels agree to within 1.0 cm^{-1} and none differ by more than 5.5 cm^{-1}. A similar comparison was made for the lowest 1932 rovibrational levels for $J = 10$. Here the average deviation between corresponding levels is 0.775 cm^{-1}. Over 90% of the levels agree to within 2.5 cm^{-1} and none disagree by more than 6.5 cm^{-1}. For $J = 10$ we also performed a calculation of the rovibrational levels using the "adiabatic rotation approximation". The average deviation between the adiabatic and exact results for the same 1932 levels is 1.737 cm^{-1}. In this case over 90% of the levels agree to within 4.5 cm^{-1} and none disagree by more than 9.5 cm^{-1}. This level of agreement is quite acceptable for present purposes but considerably weaker than that between exact results and the approximate fit we have advocated above. The current approximation scheme proves superior to the adiabatic rotation approximation, presumably because in an indirect way, the state-specific rotational constants incorporate the (weak) Coriolis coupling which is neglected in the "adiabatic rotation approximation".[19b]

Limitations of our computational resources precluded performing such tests of the approximate rovibrational spectrum for HCO_2. The greater width of the A_i and B_i distributions for HCO_2 (as compared to $H\cdots CO_2$) suggests that rotation−vibration interactions may be stronger in HCO_2 than in the transition state, and therefore, the approximate separable fit may not be as accurate in this case. However, it is important to recall the use to be made of these spectra, i.e., generation of an estimate of the density of rovibrational states for fixed J, and therefore, they need not be of spectroscopic accuracy.

In studies of the dissociation of symmetric top molecules with $J > 0$, a quantity of prime interest is the K-averaged rate constant (since except for small molecules K quantum numbers are usually experimentally unresolved) given by

$$k(E, J) = \frac{\sum_{K=-J}^{J} N^{\ddagger}[E - \epsilon^{\ddagger}_{n,J,K}]}{\sum_{K=-J}^{J} \rho(E,J,K)} \equiv \frac{N^{\ddagger}_{J}(E)}{\rho_{J}(E)} \qquad (15)$$

where in analogy to eq 1, $N^{\ddagger}[E - \epsilon^{\ddagger}_{n,J,K}]$ is the sum of rovibrational states for the transition state with specified J,K values up to energy E (measured relative to the reagent ZPE level) and $\rho(E,J,K)$ is the J,K-specific density of rovibrational states of the reagent. Summing over K we obtain $N^{\ddagger}_{J}(E)$, the sum of rovibrational states of the transition state with a specified J value up to energy E, and $\rho_J(E)$, the density of rovibrational states of the reagent with a specified value of J at energy E. Accurate evaluation of these two quantities requires an accurate determination of the rovibrational energy levels of the reactant molecule and of the transition state.

We have modeled the rovibrational spectrum in three ways that are based on eq 14 and hence assumed an approximate separation of rotation and vibration. In two cases we have taken $E^{(i)}_{J=0}$ to be derived from 3-MR results (for consistency) obtained using MULTIMODE for both HCO_2 and the $H\cdots CO_2$ transition state; in the third case, the standard RRKM expression for $E^{(i)}_{J=0}$ as a sum of separable harmonic NM energies has been used. The two MULTIMODE-based models differ with respect to the rotational constants used in generating $\Delta E^{(i)}_{J,K_a}$. In the more detailed model denoted MMSS, state-specific rotational constants (obtained as described above) were used for all relevant vibrational states of the reagent and of the transition state. In the less detailed model denoted as MMAV, all vibrational states of each species are assigned the corresponding ensemble average values $\langle A_i \rangle$ and $\langle B_i \rangle$. In the standard RRKM model denoted as RRHO, the rotational constants for all states of each species are taken to be those determined at the equilibrium geometry of that species.

These spectra were then used to generate $N^{\ddagger}_{J}(E)$ and $N_J(E)$ for $H\cdots CO_2$ and HCO_2, respectively, by direct count. In the 3000 cm^{-1} range just above the $J = 0$ threshold, $N_J(E)$ for each model was fit to a cubic polynomial for each J value up to $J = 99$, and these expressions were differentiated to obtain analytical quadratic polynomial expressions for the $\rho_J(E)$. These results were then used in eq 15 to obtain $k(E,J)$ values for $0 \le J \le 99$ and E approximately in the range of 3500−6500 cm^{-1}.

Typical results for $k(E,J)$ are presented in Figures 9 and 10. Figure 9 shows $k(E,J)$ versus J for an energy 3000 cm^{-1} above the $J = 0$ threshold. The observant reader will note that the $J = 0$ MMSS and MMAV results in Figure 9 are about 10% higher than those shown in Figure 5. This difference arises because to be consistent with our $J = 1$ calculations and our fitting of A_i and B_i we have used the results of a 3-MR $n_{max} = 9$ calculation here to obtain $\rho_J(E)$, whereas the data of Figure 5 were obtained using the results of a 3-MR $n_{max} = 10$ calculation for $\rho(E)$. The greater value of $k(E,J=0)$ in Figure 9 is a direct reflection of the reduced value of $\rho_{J=0}(E)$ obtained from the 3-MR $n_{max} = 9$ results and used in these calculations. Thus the discrepancy between the RRHO results and the nonseparable results for $k(E,J)$ is probably greater than reflected in Figure 9. The large gap between the RRHO and two sets of MM results seen in Figure 9 (until the rapid falloff at large J) primarily reflects the difference in vibrational spectra ($E^{(i)}_{J=0}$) between the two models. Differences arising due to the different treatments of rotation ($\Delta E_{J,K_a}{}^{(i)}$) are much less significant. This conclusion is supported by the observation that the differences between the two sets of MM-based results, one using state-specific rotational constants (MMSS) and the other using a fixed pair of average constants (MMAV) are minor (an order of magnitude smaller than the difference of either with the RRHO results) by comparison. The difference between these two sets of results is negligible until J exceeds 25. For lower energies than the one shown in Figure 9, the behavior of the three sets of $k(E,J)$ results are qualitatively similar, though as might be expected from Figure 5, the gap between the RRHO- and MM-based results narrows as E decreases.

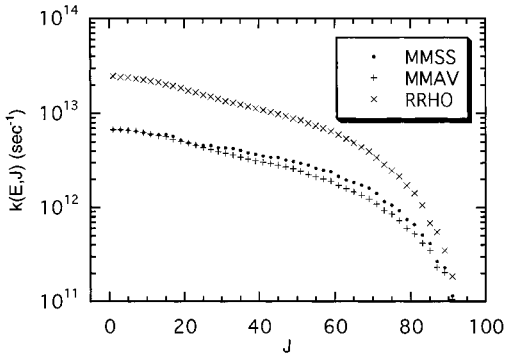

Figure 9. Comparison of RRHO, MMSS, and MMAV K-averaged unimolecular rate constants $k(E,J)$ for $HCO_2 \rightarrow H + CO_2$ dissociation versus J for a fixed energy 3000 cm^{-1} above the $J = 0$ threshold.

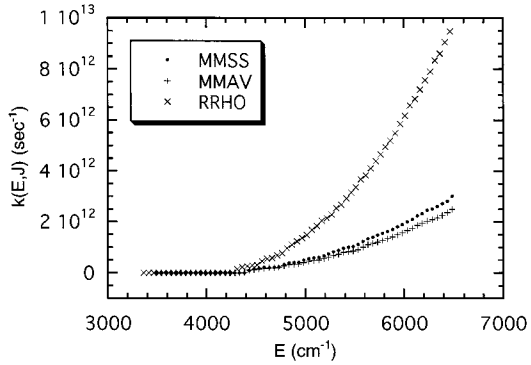

Figure 10. Comparison of RRHO, MMSS, and MMAV K-averaged unimolecular rate constants $k(E,J)$ for $HCO_2 \rightarrow H + CO_2$ dissociation as a function of energy for $J = 50$.

Figure 10 shows $k(E,J)$ versus E for $J = 50$. For this value of J the reaction threshold has shifted upward approximately 900 cm^{-1} compared to $J = 0$. As a result, at a fixed total energy E, $k(E,J = 50)$ is substantially less than $k(E,J = 0)$ for all three models. Again most of the difference seen here between the RRHO- and the MM-based results is attributable to the differences in the $J = 0$ vibrational spectra used in these models. In the energy range examined, the MMAV and MMSS results

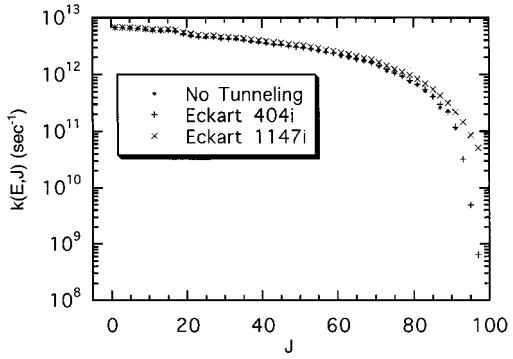

Figure 11. Comparison of MMSS K-averaged unimolecular rate constants $k(E,J)$ for $HCO_2 \rightarrow H + CO_2$ dissociation with and without separable Eckart tunneling correction versus J at an energy 3000 cm^{-1} in excess of the $J = 0$ threshold.

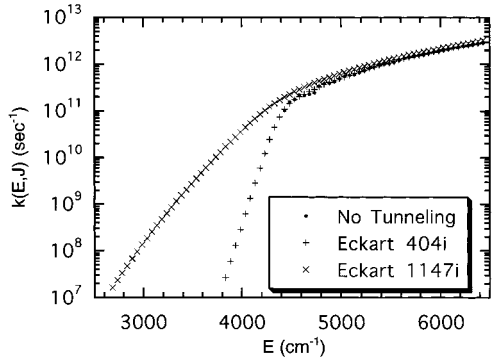

Figure 12. Comparison of MMSS K-averaged unimolecular rate constants $k(E,J)$ for $HCO_2 \rightarrow H + CO_2$ dissociation with and without separable Eckart tunneling correction as a function of energy for $J = 50$.

show a slow divergence with increasing energy, a behavior typical for J values in excess of 25.

We can incorporate tunneling effects into the calculation of $k(E,J)$ using the same approximation of a separable Eckart potential along the reaction coordinate as described earlier for the $J = 0$ case. Typical results for $k(E,J)$ using MMSS data and incorporating this approximate treatment of tunneling are shown in Figures 11 and 12. In each figure results obtained in the absence of tunneling are compared to results obtained including tunneling effects approximately using the two ω_b values as before, 404 and 1147 cm^{-1}. Figure 11 shows $k(E,J)$ versus J for a fixed energy identical to that used in Figure 9, and Figure 12 shows $k(E,J)$ versus E for $J = 50$ (the same value used in Figure 10). The most notable effect of tunneling at fixed energy seen in Figure 11 is to extend the range of J values for which dissociation can occur with an appreciable rate. For the case of the narrower barrier ($\omega_b = 1147$ cm^{-1}) even below the maximum classically allowed value of J ($J = 91$) a modest but discernible enhancement of $k(E,J)$ due to tunneling can be seen in this figure. For the broader barrier ($\omega_b = 404$) on the scale of this figure, the effects of tunneling are almost imperceptible in the range of classically accessible J. The data in Figure 11 are representative for energies well above the ZPE level of the transition state. Of course, at lower energies (near or below the ZPE level of the transition state) tunneling becomes the dominant mode of dissociation for all J. The most striking features of Figure 12 are the significant rates of tunneling-induced dissociation, even several hundred wavenumbers below the classical threshold. Just above the classical threshold there are some modest enhancements to the rate due to tunneling contributions as well, but these appear to be becoming less significant with increasing energy. As the reader may have deduced from the qualitative similarity of the data in Figures 5 and 12, the data shown in those figures are qualitatively representative of $k(E,J)$ data for other J values as a function of the energy.

IV. Summary and Conclusions

We reported unimolecular dissociation rates for $HCO_2 \rightarrow H + CO_2$ for zero and nonzero total angular momentum, using a nonseparable version of RRKM theory. The calculations of the density of states of the HCO_2 reactant and of the number of states of the transition state were done using the code MULTIMODE, and the main objective of these calculations was to assess the accuracy of standard, separable RRKM theory. The calculations for the nonseparable Hamiltonian using MULTIMODE were based on the exact Watson Hamiltonian, but with a hierarchical mode representation of the full potential. Calculations were done using 3- and 4-mode representations of the potential. The good agreement of the energies for these representations for HCO_2 and the $H\cdots CO_2$ transition state gave us confidence in the accuracy of these calculations. Exact and approximate calculations of rovibrational energy levels were also done for low values of the total angular momentum J.

The density of states of HCO_2 was obtained from an analytical fit of the energy spectrum from our largest ($n_{max} = 10$) 3-MR calculation. This expression was then used with a direct count of the nonseparable states of the transition state to obtain the dissociation rate constant for $J = 0$ over a range of total energies up to 3000 cm^{-1} above the classical dissociation threshold. Analogous calculations were also done in the separable harmonic approximation.

One important difference between the nonseparable and separable calculations was in the $J = 0$ classical threshold energy for dissociation. The classical threshold energy for dissociation, i.e., the difference in the zero-point energies of the transition state and of HCO_2, was found to be about 120 cm^{-1} higher in the accurate nonseparable calculation than in the harmonic separable one. This was due primarily to a large difference in the transition state zero-point energies, with the nonseparable calculation giving a ZPE about 250 cm^{-1} higher than the one from the separable harmonic calculation. This difference in transition state zero-point energies combines with a separable harmonic overestimate of the CO_2 reactant ZPE by about 50 cm^{-1} to produce a 300 cm^{-1} difference between the separable harmonic and accurate nonseparable threshold energies for the $H + CO_2$ association reaction.

Additionally it was found that HCO_2 exhibited typical molecular behavior in that the separable harmonic approximation significantly underestimated the density of vibrational states at energies above the dissociation threshold. This effect, combined with an overestimate of the sum of vibrational states of the transition state in the separable harmonic approximation (and the threshold effect noted above), produced separable harmonic dissociation rate constants for $J = 0$ that differed by as much as a factor of four from accurate nonseparable rate constants in the energy range considered.

Calculations of the unimolecular rate constant for J greater than zero were presented. One used state-specific rotational constants. These were obtained by fitting the difference in energies for exact $J = 1$ results relative to $J = 0$ results to the expression for a prolate symmetric top (which was shown to be appropriate for both HCO_2 and $H\cdots CO_2$). Another, more approximate, calculation used average rotational constants and was found to be in reasonably good agreement with the more accurate one, based on state-specific rotational constants.

Tunneling was incorporated into calculations of the unimolecular rate constants for $J \geq 0$ assuming a separable Eckart potential along the reaction coordinate. Tunneling was found to produce significant dissociation rates well below the *J*-dependent classical threshold energies. Within this model, the extent of tunneling was found to be strongly dependent on the potential curvature of the barrier, a quantity which has varied considerably in the various versions of the HCO_2 potential.

Quantitative application of RRKM theory requires an accurate evaluation of the molecular density of states and of the number of states of the transition state. As has been shown for the tetraatomic HCO_2 system, accurate determination of these quantities, which requires inclusion of the effects of anharmonicity and intermode coupling, is within reach of current computational resources. With future developments in computer hardware, it can be expected that studies of this type will be extended to larger systems.

Acknowledgment. K.M.C. thanks the Cherry L. Emerson Center for Scientific Computation for a visiting fellowship and Augustana College for a sabbatical leave, both of which provided support during the time this work was completed. We thank George Schatz and Kimberly Bradley for sending the HCO_2 potential. J.M.B. thanks the Department of Energy (DE-FG02-97ER14782) for support of this work.

References and Notes

(1) Bowman, J. M.; Schatz, G. C. *Annu. Rev. Phys. Chem.* **1995**, *46*, 169.

(2) Zhang, J. Z. H.; Dai, J.; Zhu, W. *J. Phys. Chem.* **1997**, *101*, 2746.

(3) (a) T. D. Sewell and D. L. Thompson, Int. J. Mod. Phys. B **1997**, *11*, 1067. (b) Mayne, H. R. In *Dynamics of Molecules and Chemical Reactions*; Wyatt, R. E., Zhang, J. Z. H., Eds.; Dekker: New York, 1996; Chapter 15.

(4) Pechukas, P. In *Dynamics of Molecular Collisions*; Miller, W. H., Ed.; Plenum: New York, 1976; Part B, Chapter 6.

(5) Truhlar, D. G.; Hase, W. L.; Hynes, J. T. *J. Phys. Chem.* **1983**, *87*, 2664.

(6) Baer, T.; Hase, W. L. *Unimolecular Reaction Dynamics*; Oxford: New York, 1996; Chapters 6 and 7.

(7) Miller, W. H. Chapter 10 of ref 3b.

(8) This work is reviewed in ref 5 as well as in the following: Truhlar, D. G.; Isaacson, A. D.; Garrett, B. C. In *Theory of Chemical Reaction Dynamics*; Baer, M., Ed.; CRC Press: Boca Raton, FL, 1985; Vol. 4, pp 66−137.

(9) (a) Isaacson, A. D.; Truhlar, D. G. *J. Chem. Phys.* **1982**, *76*, 1380; (b) Truhlar, D. G.; Isaacson, A. D.; Skodje, R. T.; Garrett, B. C. *J. Phys. Chem.* **1982**, *86*, 2252. Erratum: *J. Phys. Chem.* **1983**, *87*, 4554.

(10) (a) Isaacson, A. D.; Hung, S.-C. *J. Chem. Phys.* **1994**, *101*, 3928; (b) Isaacson, A. D. *J. Chem. Phys.* **1997**, *107*, 3832.

(11) (a) Christoffel, K. M.; Bowman, J. M. *Chem. Phys. Letters* **1982**, *85*, 220; (b) Romanowski, H.; Bowman, J. M. *Chem. Phys. Letters* **1984**, *110*, 235.

(12) (a) Miller, W. H.; Hernandez, R.; Handy, N. C.; Jayatilaka, D.; Willetts, A. *Chem. Phys. Lett.* **1990**, *172*, 62; (b) Cohen, M. J.; Handy, N. C.; Hernandez, R.; Miller, W. H. *Chem. Phys. Lett.* **1992**, *192*, 407; (c) Cohen, M. J.; Willetts, A.; Handy, N. C. *J. Chem. Phys.* **1993**, *99*, 5885.

(13) Seideman, T.; Miller, W. H. *J. Chem. Phys.* **1991**, *95*, 1768.

(14) See ref 6, p.8.

(15) Forst, W. *Chem. Revs.* **1971**, *71*, 339.

(16) Peslherbe, G. H.; Hase, W. L. *J. Chem. Phys.* **1994**, *101*, 8535.

(17) Song, K.; Peslherbe, G. H.; Hase, W. L.; Dobbyn, A. J.; Stumpf, M.; Schinke, R. *J. Chem. Phys.* **1995**, *103*, 8891.

(18) Bradley, K. S.; Schatz, G. C. *J. Chem. Phys.* **1997**, *106*, 8464. This surface is based on modification of earlier surfaces presented: (a) Schatz, G. C.; Fitzcharles, M. S.; Harding, L. B. *Faraday Disc. Chem. Soc.* **1987**, *84*, 359; (b) Kudla, K.; Schatz, G. C.; Wagner, A. F. *J. Chem. Phys.* **1991**, *95*, 1635.

(19) (a) Carter, S.; Culik, S. J.; Bowman, J. M. *J. Chem. Phys.* **1997**, *107*, 10458; (b) Carter, S.; Bowman, J. M. *J. Chem. Phys.* **1998**, *108*, 4397; (c) Carter, S.; Bowman, J. M.; Handy, N. C. *Theo. Chem. Accts.* (in press).

(20) Tennyson, J. *J. Chem. Soc. Faraday Trans.* **1992**, *88*, 3271.

(21) Watson, J. K. G. *Mol. Phys.* **1968**, *15*, 479.

(22) Whitehead, R. J.; Handy, N. C. *J. Mol. Spectrosc.* **1975**, *55*, 356.

(23) Bowman, J. M. *Chem. Phys. Lett.* **1994**, *217*, 36.

(24) (a) Bowman, J. M. *Acc. Chem. Res.* **1986**, *19*, 202; (b) Gerber, R. B.; Ratner, M. A. *Adv. Chem. Phys.* **1988**, *70*, part 1, 97.

(25) Bowman, J. M.; Shnider, H. *J. Chem. Phys.* **1999**, *110*, 4428.

(26) See ref. 6, Chapter 7 and references therein.

(27) Miller, W. H. *J. Am. Chem. Soc.* **1979**, *101*, 6810.

(28) (a) Eckart, C. *Phys. Rev.* **1930**, *35*, 1303; (b) Johnston, H. S. *Gas Phase Reaction Rate Theory*; Ronald Press: New York, 1966; pp 40−47.